Accepted Manuscript

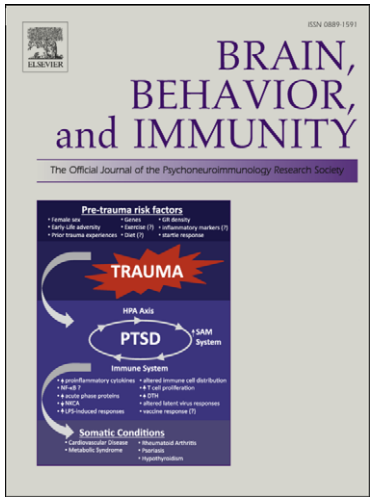

Age-related changes in the hippocampus (loss of synaptophysin and glial-synaptic interaction) are modified by systemic treatment with an NCAM-derived peptide, FGL

Bunmi Ojo, Payam Rezaie, Paul L. Gabbott, Heather Davies, Frances Colyer, Thelma R. Cowley, Marina Lynch, Michael G. Stewart

PII: S0889-1591(11)00531-9
DOI: 10.1016/j.bbi.2011.09.013
Reference: YBRBI 1849

To appear in: *Brain, Behavior, and Immunity*

Please cite this article as: Ojo, B., Rezaie, P., Gabbott, P.L., Davies, H., Colyer, F., Cowley, T.R., Lynch, M., Stewart, M.G., Age-related changes in the hippocampus (loss of synaptophysin and glial-synaptic interaction) are modified by systemic treatment with an NCAM-derived peptide, FGL, *Brain, Behavior, and Immunity* (2011), doi: 10.1016/j.bbi.2011.09.013

Age-related changes in the hippocampus (loss of synaptophysin and glial-synaptic interaction) are modified by systemic treatment with an NCAM-derived peptide, FGL

Bunmi Ojo[a], Payam Rezaie[a], Paul L. Gabbott[a], Heather Davies[a], Frances Colyer[a], Thelma R. Cowley[b], Marina Lynch[b], Michael G. Stewart[a]*

[a]Department of Life Sciences, The Open University, Walton Hall, Milton Keynes MK7 6AA, UK;
[b]Trinity College Institute of Neuroscience, Trinity College, Dublin 2, Ireland.

Running Title: FGL modifies age-related changes in the hippocampus

***Correspondence to:**

Michael G. Stewart PhD
Professor of Neuroscience
Department of Life Sciences
The Open University
Walton Hall
Milton Keynes
MK7 6AA, United Kingdom
Tel +44-1908 653448
Fax+ 44-1908 654167
E-mail: m.g.stewart@open.ac.uk

Grant sponsor: Supported by the European Union FPVI "Promemoria" programme grant (Contract No. 512012) and FP7 'MemStick' (Ref: 201600)

Abstract

Altered synaptic morphology, progressive loss of synapses and glial (astrocyte and microglial) cell activation are considered as characteristic hallmarks of ageing. Recent evidence suggests that there is a concomitant age-related decrease in expression of the presynaptic protein, synaptophysin, and the neuronal glycoprotein CD200, which, by interacting with its receptor, plays a role in maintaining microglia in a quiescent state. These age-related changes may be indicative of reduced neuroglial support of synapses. FG Loop (FGL) peptide synthesised from the second fibronectin type III module of neural cell adhesion molecule (NCAM), has previously been shown to attenuate age-related glial cell activation, and to 'restore' cognitive function in aged rats. The mechanisms by which FGL exerts these neuroprotective effects remain unclear, but could involve regulation of CD200, modifying glial-synaptic interactions (affecting neuroglial 'support' at synapses), or impacting directly on synaptic function. Light and electron microscopic (EM) analyses were undertaken to investigate whether systemic treatment with FGL (i) alters CD200, synaptophysin (presynaptic) and PSD95 (postsynaptic) immunohistochemical expression levels, (ii) affects synaptic number, or (iii) exerts any effects on glial-synaptic interactions within young (4 month-old) and aged (22 month-old) rat hippocampus. Treatment with FGL attenuated the age-related loss of synaptophysin immunoreactivity (-ir) within CA3 and hilus (with no major effect on PSD-95-ir), and of CD200-ir specifically in the CA3 region. Ultrastructural morphometric analyses showed that FGL treatment (i) prevented age-related loss in astrocyte-synaptic contacts, (ii) reduced microglia-synaptic contacts in the CA3 stratum radiatum, but (iii) had no effect on the mean number of synapses in this region. These data suggest that FGL mediates its neuroprotective effects by regulating glial-synaptic interaction.

Key words: Ageing, hippocampus, CA3, astrocytes, microglia, CD200, synaptophysin, PSD-95, morphometric analysis, immunoelectron microscopy

1. Introduction

Synapses are formed by functional contact between axons in close apposition with postsynaptic terminals of their target neurons. Persistent changes in synaptic efficacy of neurons within the hippocampus result in long term potentiation (LTP) and this is believed to provide a basis for the storage of memory in the brain (Bliss and Collingridge 1993). The close proximity of synaptic contacts to neuroglial (astrocyte and microglial) cell processes is vital in supporting synaptic function/activity (Barres, 2008; Paixao and Klein, 2010; Schultz et al., 1957). Astrocytic processes located at the synapse are known to communicate actively with the pre- and post-synaptic elements of neuronal terminals influencing a variety of synaptic functions (Giaume et al., 2010). Microglial cells are also involved in synaptic function, supplying neurotrophic factors and selectively removing degenerating synapses as a protective mechanism (Cullheim and Thams, 2007; Farber and Kettenmann, 2005; Trapp et al., 2007). Diminished neuroglial support at the synapse is therefore likely to alter synaptic 'connectivity' and consequently impact on cognitive capability.

One of the characteristic hallmarks of ageing is a deficit in cognitive function, which especially in the hippocampus correlates with altered synaptic morphology including loss of pre-post/synaptic structural proteins (such as synaptophysin and PSD95 respectively) and progressive loss of synaptic density, (Burke and Barnes, 2006; Driscoll et al., 2006; Rapp and Gallagher, 1996; Rosenzweig and Barnes, 2003). These changes are associated with an underlying neuroinflammatory response, typified by neuroglial activation and increased pro-inflammatory cytokine production (Godbout et al., 2005; Lyons et al., 2009). It has been proposed that the maintenance of neuroglial cells in a non-inflammatory ('quiescent') state could be an important determining factor for preserving synaptic function (Piazza and Lynch, 2009) minimising the heightened vulnerability of the brain in ageing.

Neuronal CD200 is a glycoprotein which interacts via cell-cell contact with its cognate receptor (CD200R) localised mainly on cells of the myeloid lineage including microglial cells (Barclay et al., 2002). Recent evidence suggests CD200R expression is present also on astrocytes (Chitnis et al., 2007). Activation of CD200R has been shown to spatially modulate the extent of glial activation, maintaining these cells in a 'quiescent' state (Lyons et al., 2007). Consistent with these findings, deficits in LTP, induced either by lipopolysaccharide (LPS) stimulation, or with 'normal' ageing, have been shown to be rescued by intra-cerebroventricular injections of CD200Fc (through its ability to ameliorate microglial activation by acting on CD200R) (Lynch, 2010). The cellular distribution of CD200 protein, and particularly its localisation between synapses has not been investigated previously. If changes in synaptic density parallel a reduction in CD200 levels with age, it is possible that this could be one mechanism contributing towards progressive neuroglial activation (i.e. reduced interaction between CD200 and CD200R on neuroglial cell processes at

synapses) that is seen with age, and may lead to loss of structural/functional support at synapses. However, differential expression of CD200 at synapses remains to be verified.

We have previously shown that a Neural Cell Adhesion Molecule (NCAM) -derived peptide, FGL, which increases CD200 *in vitro* and *in vivo*, can act as a novel anti-inflammatory agent in models of ageing and age-related diseases, restoring cognitive function and ameliorating neuropathological changes (Cambon et al., 2004; Downer et al., 2010; Klementiev et al., 2007; Neiiendam et al., 2004; Popov et al., 2008; Skibo et al., 2005; Stewart et al., 2010). The present study examined whether FGL modulates age-related changes within the hippocampus. Specifically, whether systemic treatment with FGL (i) alters CD200, synaptophysin (presynaptic) and PSD95 (postsynaptic) expression levels, (ii) affects synaptic density, or (iii) modifies glial-synaptic interactions within the hippocampus of young (4 month-old) and aged (22-month-old) rats.

2. Methods

2.1. Animals

Male Wistar rats (Trinity College, Dublin, Ireland) aged 4 months (250-350g) or 22 months (450–550 g) were housed in pairs under a 12-hr light schedule at ambient temperature controlled between 22˚C and 23˚C. Animals were maintained under veterinary supervision throughout the study. There was no evidence of disease amongst the colony and healthy (young and aged) rats were used in this study. Experiments were performed under a license issued by the Department of Health (Ireland) and in accordance with the guidelines approved by the local ethical committee at Trinity College Dublin.

2.2. Treatment

Animals were injected subcutaneously with 8 mg ⁄ kg FGL_L (5 mg/ml solution in sterile water) or with the same volume of vehicle (sterile water), on alternate days, receiving 10 doses in total, the first on experimental Day 1 and the last on Day 19. The FGL_L peptide was sourced from Polypeptide Laboratories (Hillerod, Denmark) (Klementiev et al., 2007). Purity was estimated by HPLC and MALDI-TOF MS (VG TOF Spec E, Fisons Instruments, Beverly, MA, USA). The injected form of the peptide (FGL_L) is a 'dimeric form' of FGL and consists of two FGL monomers linked at the N-terminal. This dimeric form was previously selected for clinical development (Anand et al., 2007). The dose and route of administration was based on previous publications (Downer et al., 2010; Secher et al., 2006). Previous studies, using the same treatment regime described here, demonstrated that FGL crossed the blood–brain barrier within 10 min of injection and remained detectable in the cerebrospinal fluid (CSF) for up to 5 hours (see for example Secher et al., 2006). Blood plasma levels of FGL were up to 10-fold higher than in CSF during the first 2

hours after administration (Secher et al., 2006). On Day 20 rats were prepared for light microscopic examination.

2.3. Tissue preparation and processing for light microscopy

Animals were deeply anesthetised with urethane (1.5 g/kg), perfused transcardially with 100mL of physiological saline, followed by 100mL of 2% paraformaldehyde and 3.75% acrolein in 0.1M phosphate buffer pH 7.4 (PB) at room temperature, and 400mL of 2% parafomaldehyde in PB. After perfusion, the brains were removed from the skull, post-fixed in 2% paraformaldehyde in PB at 4°C and stored in 0.1M phosphate buffer solution. Forebrain blocks, which included the dorsal anterior hippocampus were marked to allow subsequent identification. Serial 50µm-thick coronal sections, cut using a Leica VT100 vibrating microtome from the left dorsal anterior hippocampus, were collected and stored at -20°C in storage solution (30% sucrose and 30% ethylene glycol in PB).

2.4. Immunohistochemical staining of rat brain sections for light microscopy

Three separate (1 in 10) series of 50µm-thick, fixed coronal sections were taken throughout the extent of the left dorsal hippocampus (bregma -1.80mm to -4.16mm; Paxinos and Watson, 2007), and immunostained in entire batches (5 animals per group), with well-characterised antibodies raised against synaptophysin (rabbit anti-synaptophysin, 1:7500, Abcam), PSD-95 (mouse anti-PSD-95, 1:400, Abcam), and CD200 (goat anti-CD200, 1:10, R&D Systems). We also tested two further reagents (mouse anti-CD200 monoclonal, 1gG2a, AbCam ab33734; mouse anti-CD200R monoclonal IgG1, AbCam ab17225), but were unable to get consistent and reliable immunohistochemical staining with these antibodies on our fixed tissue samples. Our immunostaining protocols were optimised before applying to batches of tissue sections (run at the same time for each immunoreagent). Briefly, tissue sections were rinsed overnight at room temperature (RT) in a solution of phosphate buffer (PB: 0.1M, pH 7.4) and treated for 30 minutes at RT with freshly made [0.26M] sodium borohydride in PB. After rinsing, sections were immersed for 1 hour in endogenous peroxidase blocking solution (10% methanol in deionised water, to which 3% hydrogen peroxide solution was added), rinsed with deionised water, and incubated with 10% normal swine serum (for synaptophysin), horse serum (for PSD-95), or rabbit serum (for CD200), containing 0.01% Tween 20, for a period of 2 hours. They were next incubated overnight with primary antibody solution made up in 1% normal rabbit/swine/horse serum with 0.01% Tween 20, on a shaker at RT. Sections were rinsed three times with PB and transferred to secondary antibody (for synaptophysin marker: biotinylated swine anti-rabbit IgG at 1:200, Dako; for PSD-95 marker: biotinylated horse anti-mouse IgG at 1:100, Vector Laboratories; for CD200 marker: biotinylated rabbit anti-goat IgG at 1:100, Dako) for 2 hours at RT. Sections were rinsed three times with PB and incubated for 1 hour at RT with avidin-biotin-horseradish peroxidase solution (Vectastain Elite

ABC kit; Vector Laboratories) in PB containing 0.01% Tween 20. After washing, immunoreactivity was visualised with 3,3'-diaminobenzidine (DAB) chromogen, and 0.05% hydrogen peroxide. Sections were processed in entire batches for each antibody marker. Development with the chromogen was timed and applied as a constant across batches to limit technical variability in immunodetection, before progressing to quantitative image analysis (see Brey et al., 2003). Finally, sections were mounted onto gelatin-coated glass slides, progressed through a graded series of alcohols, cleared in xylene and cover slipped with PerTex mounting medium. Negative control sections were included where the primary antibody was omitted and replaced either with blocking serum (10% normal swine, horse or rabbit serum) or biotinylated secondary antibodies alone (swine anti-rabbit, horse anti-mouse or rabbit anti-goat). Immunoreacted sections were viewed with a Nikon Microphot-FX microscope (Nikon UK Ltd).

2.5. Quantitative image analysis of synaptophysin, PSD-95 and CD200 immunoreactivity

Immunoreactivity for synaptophysin, PSD-95 and CD200 (see Figure 1) was measured by quantitative image analysis (optical segmentation) using Image-Pro Plus software (Media Cybernetics, Europe), as previously described (Leuba et al., 1998; Milnerwood et al., 2006; Pontikis et al., 2004; Rezaie et al., 2005) with each marker analysed blind with respect to grouping. Quantitative immunohistochemistry, using computerised image analysis and optical segmentation techniques (or 'densitometric' analysis), is an established procedure used in modern clinical and experimental histopathology (Brey et al., 2003; Campuzano et al., 2008; Kokolakis et al., 2008; Peretti-Renucci et al., 1991; Wang et al., 2009; Zehntner et al., 2008), with strong test-retest reliability, that allows comparative analysis of immunostained sections (captured as images) to be made in different laboratories (Brey et al., 2003; Dobson et al., 2010). Commercially available image analysis programmes, such as used here (see Xavier et al., 2005), are an aid to standardise interpretation. A correlation between immunohistochemical staining and protein levels has also been shown independently using Western blot and immunoassays (see Brey et al., 2003). There are a number of ways to measure the 'level' of immunohistochemical stain (Brey et al., 2003). In this study we examined the area of tissue stained with DAB (percent area), defined as the area of the image classified as stained with DAB, divided by the total image area. Given that nuclear stains often confound the results of imaging techniques, the 'pure' DAB stain was analysed giving optimal results (see Figure 1A-F). We applied rigorous staining protocols, outlined above, to ensure consistency of immunostaining, and accuracy of image analysis.

Immunoreactvity was specifically assessed within the dentate gyrus, hilus, CA3 and CA1 (spanning the stratum pyramidale, partially the stratum radiatum) subfields of the hippocampus (Paxinos and Watson, 2007). A survey of immunoreacted tissue sections was performed independently to verify specific immunoreactivity in each series of sections subsequently progressed to quantitative image

analysis. Briefly, non-overlapping RGB images were digitally captured at random within the defined areas from each section in the series, providing a systematic survey throughout each region of the dorsal hippocampus for each animal within a group. Images were captured via a digital camera (JVC KY-F75V) mounted onto a Nikon Microphot-FX microscope (Nikon UK Ltd) using a x40 objective and neutralizing grey filters. All parameters including the lamp intensity, digital camera setup, microscope and video calibration were held constant. A minimum of 20 microscopic fields were analysed per region, per animal. Individual microscopic fields measured 150µm x 112µm, giving a total area of 1.68mm^2 examined for each subfield per group (n=5 animals per group). Optical segmentation of immunoreacted profiles was analysed using Image-Pro Plus morphometric image analysis software (version 5.0, Media Cybernetics) as previously described (Milnerwood et al., 2006; Pontikis et al., 2004; Rezaie et al., 2005). A semi-automated RGB histogram-based protocol (specified in the image analysis programme) was employed to determine the optimal segmentation (threshold setting) for immunoreactivity for each antibody. The specificity of the detection method was also verified manually by monitoring the analysis as it progressed, per region, per animal. Macros were subsequently recorded to transfer the data to a spreadsheet for subsequent statistical analysis. Data were separately plotted as the mean percentage area of immunoreactivity per field (denoted "% Area") ± SEM for each region and grouping.

2.6. Electron microscopy (EM)

2.6.1. Pre-embedding single immunolabelling of rat brain sections

Three separate series of sections (50µm-thick) were taken from the left dorsal hippocampus, and immunostained with antibodies raised against GFAP (rabbit anti-GFAP at 1:1000, Abcam), IBA-1 (goat anti-IBA-1 at 1:100, Abcam), and CD200 (goat anti-CD200 at 1:10, R&D systems); one antibody per series. All sections were treated for 30 minutes with [0.26M] sodium borohydride. After rinsing copiously with PB, sections were permeabilised with 0.05% triton X-100 in PB (0.1M, pH 7.4). Following permeabilisation, sections were incubated in either 10% normal swine serum (for GFAP), or 10% normal rabbit serum (for IBA-1 and CD200), containing 0.01% Tween 20 for a period of 2 hours, transferred to primary antibody solution made up in 1% normal swine (for GFAP) or rabbit serum (for IBA1/CD200) containing 0.01% Tween 20 and subsequently incubated overnight on a shaker at RT. From this stage onwards, these sections underwent the same immunostaining protocol already described (see in section 2.4) using the electron-dense DAB as chromogen. Negative control sections were included where the primary antibody was omitted and replaced either with blocking serum (10% normal swine or rabbit serum) or biotinylated secondary antibodies alone (swine anti-rabbit or rabbit anti-goat).

2.6.2. Processing for EM

Sections were processed for electron microscopic analysis as previously described (Popov et al., 2008). Briefly, 50µm-thick whole hippocampal slices were post-fixed in 2% osmium tetroxide diluted in PB for 1 hour at RT. Sections were dehydrated in graded aqueous solution of acetone and infiltrated with a (50:50) solution mixture of 100% acetone and Epon overnight in capped vials at RT. These were infiltrated in Epon for 2 hours in uncapped vials and subsequently sandwiched between two sheets of Aclar film (Agar Scientific). Capsules of Epon were placed over the area required in the slice and polymerised at 60°C for 48 hours. Epon blocks were coded and further analyses were carried out blind to the experimental status of the tissue. Slices embedded on the surface of resin blocks were trimmed to isolate the area of interest (CA3 subfield extending from the pyramidal cell layer to the stratum radiatum (SR)). A Leica UCT ultramicrotome with diamond knife was used to obtain ultrathin serial sections (60-70 nm thick) from the area of interest, and collected on formvar-coated copper slot grids. Sections were counterstained with uranyl acetate, followed by Reynolds lead citrate, prior to image acquisition using an AMTXR60 digital camera attached to a JEM 1400 transmission electron microscope (8000x magnification).

2.6.3 Analysis of synaptic density within the CA3-SR

Sections from the CA3-SR were analysed (approximately 200µm from the proximal edge of the pyramidal cell layer). Non-overlapping images were digitally captured from the neuropil of the CA3-SR, to provide a random systematic survey throughout the area of interest for each animal within a group. A minimum of 40 microscopic fields (10505 x 6811nm) were analysed per animal, each field measuring 71.5µm² (at 8000x magnification), giving a total area of 14300µm^2 examined per group (n=5 animals per group). Ultrastructural characteristics, defined according to criteria described by Peters et al. (1999), were used to identify axo-spinous, asymmetric synapses with recognized postsynaptic densities (PSDs), postsynaptic spine, and a pre-synaptic component with two or more vesicles (see Figure 2). Synaptic density was calculated as the mean number of synapses per 100µm^2.

2.6.4. Analysis of glial-synaptic contacts and the surface area of glial cell processes

A minimum of 40 non-overlapping microscopic fields (10505 x 6811nm) of the CA3-SR were analysed per animal, each field measuring 71.5µm² (at 8000x magnification), giving a total area of 14300µm^2 examined per group (n=5 animals per group). Astrocytes and their processes were identified by electron dense GFAP+ stain (see Figure 3A). Microglia and their processes were identified by electron dense IBA1+ stain (see Figure 4A,B,C). Mean number of astrocyte- and microglial-synaptic contacts, glial 'perimeter' coverage of both pre and/or postsynaptic elements of the synapse, and mean surface area of astrocyte and microglial processes were determined from the same series of digital images, in a similar manner to that previously described (Jones and Greenough., 1996; Trapp et al. 2007; Tremblay et al. 2010). An areal density value was obtained for

number of astrocyte- and microglial-synaptic contacts (based on criteria mentioned above), and plotted as mean number of glial-synapse contacts per 100μm² (± SEM) (Figures 3 and 4). The perimeter coverage of synaptic elements (by astrocyte and microglial cell processes; length/nm) was manually outlined by tracing round the membrane area of the glia-synapse interface (see for example Figure 3B) using a stylus pen and digital tablet (version 5.0, Media Cynernetics), as previously described (Jones and Greenough, 1996). A pilot study determined that a minimum of 100 'contacts' was sufficient in order to ensure a CE of <0.05 (an average of 125-230 glial-synaptic contacts were examined within the CA3-SR per animal, in this study). Macros were recorded to transfer the measurement data to an Excel spreadsheet for subsequent statistical analysis. Data were plotted as the mean glial coverage of synapses (in nm ± SEM). To obtain the surface area of glial cell processes, an areal boundary was carefully drawn around each immunostained process from the same series of images used above. Data were plotted as the mean surface area of processes per 100μm² ± SEM.

2.6.5. Analysis of the cellular distribution of CD200-immunolabelled profiles

CD200-immunolabelled profiles were examined by electron microscopy. A mimimum of 40 CA3-SR microscopic fields were analysed per animal, each field measuring 71.5μm² (at 8000x magnification), giving a total area of 14300μm^2 examined per group (n=5 animals per group). The immunoperoxidase labelling was easily identifiable as dense patches of reaction product and labelled profiles were classified as boutons, axons, dendrites, spines or glial cell processes according to their morphological features as defined by Peters et al. (1991). To determine the distribution of CD200 positive profiles per 100μm², analysis was exclusively performed on the most superficial portion of tissue in contact with the Epon-resin embedded capsule where greater densities of immunolabelled profiles are seen (Peddie et al., 2008; Rodriguez et al., 2005). This potentially minimised any artificial differences in labelling attributed to penetration of antisera and immunoreagents. Mean percentage of each of the immunolabelled profiles was calculated, and data plotted as mean % distribution per 100μm² ± SEM.

2.7. Statistical analysis

Graphs were prepared using Prism 5.0 software, and data analysed using the Statistical Package for the Social Sciences program (SPSS version 17, SPSS Inc., Chicago, USA). One-way analysis of variance (ANOVA) was used with criterion $p<0.05$ to assess group differences, followed by Tukey's unequal N honest significant differences test. Data are expressed as mean ± SEM.

3. Results

3.1. Ageing is associated with a reduction in synaptophysin, PSD-95 and CD200 immunoreactivity (-ir) within the dorsal hippocampus: differential responses and FGL effects

An optical segmentation procedure was used to examine quantitatively the patterns of immunoreactivity for the synaptic markers synaptophysin (Figure 1A,B,G) and PSD-95 (Figure 1C,D,H), and for CD200 (Figure 1E,F,I) within different hippocampal subfields in young (4 month-old) and aged (22 month-old) rats treated with vehicle or FGL. Synaptophysin-ir (presynaptic protein marker) was reduced within all subfields in aged compared to young vehicle-treated animals (Figure 1G). Comparatively low levels of synaptophysin-ir were detected in the CA1 area (Figure 1A,G) and DG (Figure 1G). By comparison, PSD-95-ir and CD200-ir were significantly reduced with age only in the CA3 and DG (Figure 1H,I). FGL treatment moderately preserved synaptophysin-ir within the CA3 and hilus (Figure 1G), and CD200-ir (I) only within the CA3, but had no major effect on PSD-95-ir (except for a small decline within the CA1 subfield) in aged (22 month-old) animals. These results indicate differential age-related responses between the CA1 and CA3 subfields of the hippocampus, and point towards selective effects of FGL within the CA3 area.

3.2 Age-related loss of axo-spinous synapses within the CA3-SR is unaffected by FGL

To investigate whether treatment with FGL (in 22 months old rats) affects synaptic density, we examined hippocampal tissue under the electron microscope. We isolated the CA3 subfield as a region of interest, for a number of reasons: (i) the CA3 is notable for displaying marked structural plasticity accompanied by loss of hippocampal function (McEwen, 1999; Sandi et al., 2003; Sousa et al., 1998); (ii) microarray studies have revealed that age-related changes in expression of genes linked with cognition are affected more in the CA3 region compared to other subfields of the hippocampus (Haberman et al., 2009); (iii) our light microscopic studies (see 3.1) indicated that FGL has selective/differential effects within the hippocampus, and with notable effect in the CA3 subfield. We specifically focused on the ascending CA3-SR to avoid thorny excrescences in the proximal apical dendrites located in the stratum lucidum/pyramidale layer; these features make it difficult to identify glial cell profiles in juxtaposition to synapses. Figure 2A shows axo-spinous synapses within the CA3-SR. There was an age-related reduction in the number of synapses in this region which remained unaltered following treatment with FGL (Figure 2B).

3.3. FGL modifies age-related glial-synaptic interactions

FGL has been shown to act as a novel anti-inflammatory agent, and to downregulate glial cell activation (Downer et al., 2010). We investigated the effect of FGL on glial-synaptic interactions by examining ultrathin immunolabelled sections of the CA3-SR under the transmission electron

microscope, using well-characterised antibodies to detect astrocytes (GFAP) and microglia (IBA1). Astrocyte and microglial processes were identified using GFAP/IBA1 immunolabelling and defined morphological characteristics (Ventura and Harris, 1999; Witcher et al., 2007) (Figure 3A and 4A). IBA1+ microglia in aged animals frequently displayed a higher content of intracellular vacuoles, phagolysosomal and electron-dense material (indicative of greater phagocytic activity, and an increased 'activation state') (compare Figure 4C to Figure 4B). Lipofuscin was also occasionally detected within astrocyte processes in aged animals (Figure 3C).

The mean surface area of astrocyte processes, and coverage of synapses (apposed to pre- and post-synaptic membrane elements) did not alter with age (Figure 3D,F), whereas the mean number of astrocyte-synaptic contacts were significantly reduced in aged animals (Figure 3E; by around 2-fold). FGL treatment further reduced astrocytic coverage of synapses (Figure 3F), but increased the mean number of astrocyte-synaptic contacts (Figure 3E) within the CA3-SR in aged animals (when compared to vehicle-treated animals). The mean surface area of microglial processes (Figure 4D) and number of microglia-synapse contacts (Figure 4E) increased significantly with age, but the microglial coverage of synapses remained unaltered (either with age, or following FGL treatment) (Figure 4F). FGL treatment significantly reduced the mean surface area of microglial processes (Figure 4D) and the mean number of microglia-synapse contacts (Figure 4E) within the CA3-SR in aged animals (when compared to vehicle-treated animals).

3.4. Cellular distribution of CD200

CD200 immunolabelling was defined on different profiles at the EM level in the CA3-SR (Figure 5). Pre-embedding, single immuno-DAB labelling was used to show selective expression of CD200 on boutons, axons, spines, dendrites and glial (astrocyte) processes (Figure 5C-H), as well as on astrocytic 'endfeet' processes and on vascular endothelium (luminal aspect of endothelial cells) (Figure 5B). CD200 labelling was present both on membranes and intracellularly, within neuronal and glial structures (Figure 5A,C-H). We quantified the distribution of CD200 labelling amongst neuronal and glial cell profiles within the CA3-SR of young (4 month) and aged (22 month) rats treated with vehicle, and with FGL at 22 months (Figure 5I). CD200 was prominently expressed on dendrites (50-75%) and on astrocytes (15-30%) (Figure 5I). By comparison, less than 12.5% of boutons, axons and spines were found to express CD200 in the CA3-SR. Aged, vehicle-treated rats showed a 15% reduction in dendrites expressing CD200, compared to young vehicle-treated animals, but the distribution in spines, axons and astrocytes was elevated slightly with age (Figure 5I). FGL treatment increased slightly the CD200+ distribution in boutons and glial cell profiles, in aged (22 month-old) animals.

4. Discussion

This study has investigated age-related changes within the hippocampus and the effects of systemic treatment with FGL on morphometric parameters: (i) immunoreactivity for pre- and post-synaptic markers (synaptophysin and PSD-95), and CD200, (ii) synaptic density, (iii) glial-synaptic interactions and (iv) cellular distribution of CD200. We demonstrate that ageing is associated with a reduction in synaptophysin-ir, PSD-95-ir and CD200-ir differentially within hippocampal subfields. FGL appears to have a selective effect within the CA3 subfield (FGL treatment moderately preserved synaptophysin-ir within the CA3 and hilus (Figure 1G), and CD200-ir (I) only within the CA3, but had no major effect on PSD-95-ir (except for a small decline within the CA1 subfield) in aged (22 month-old) animals). We have further demonstrated contrasting glial-synaptic responses: a reduction in astrocyte-synaptic contacts, and an increase in microglia-synaptic contacts, with age within the CA3-SR, which are modified by treatment with FGL. This indicates that the FGL peptide may be acting through FGFR to maintain neuroglial cells in a non-inflammatory (quiescent) state thereby regulating their subsequent effects on age-related changes in synaptic parameters.

4.1. FGL effect on synaptic markers (synaptophysin and PSD-95) with age

Loss of synaptic integrity may be an integral part of cognitive decline, associated with hippocampal function. In age-related conditions such as Alzheimer's disease (AD), the degree of dementia appears to correlate with loss of synapses and may represent one of the early aspects of the disease. In aged animals synaptic density (Geinsiman, 1999, Geinisman, et al., 1992, 2004; Scheff and Price, 2006) is reduced and accompanied by disruption in synaptic function and integrity. We also found a significant reduction in synaptic density in the CA3-SR with age (Figure 2B). The synapse may thus represent one of the most susceptible components to succumb to the ageing process (rather than gross neuronal cell loss *per se*). FGL has been shown to restore cognitive impairments and deficits in synaptic function in several *in vivo* behavioural models (Cambon et al., 2004; Klementiev et al., 2007; Secher et al., 2006). In our study, synaptophysin-ir was significantly reduced in all hippocampal subfields of aged animals (Figure 1G). Consistent with this result, a significant decline in synaptophysin levels has been correlated with deficits in spatial memory in aged rats (Bondareff and Geinisman, 1976; Geinisman et al, 1986). Synaptophysin is an essential membrane protein of synaptic vesicles localised throughout the brain (Navone et al., 1986). It is known to be involved in functions such as calcium binding (Rehm et al., 1986) exocytosis (Alder et al., 1992; Mullany and Lynch 1998) and synaptic vesicle recycling (Evans and Cousin 2005). The ability of FGL to restore synaptophysin-ir to the level in younger animals within the CA3 and hilus, indicates its potential in preserving synaptic function in aged animals. This effect could be mediated directly through binding of FGL to FGF receptors (primarily FGFR1 and FGFR2) on neurons (Gonzalez et al., 1995), since the FGFR ligand FGF-2 (bFGF) has been shown to increase functional excitatory

synapses on rat hippocampal neuronal cultures *in vitro* as determined by counting puncta immunostained for synaptophysin (Li et al ., 2002). This suggests a role for FGFR as a means for controlling FGL-mediated upregulation of synaptophysin immunoreactivity with ageing. Indeed FGF-2 is known to act through the Ras/Raf/mitogen-activated protein kinase (MAPK) pathway, which has a crucial role in growth factor activity, synaptic plasticity and synaptogenesis in the CNS (Cuadrado and Nebrada, 2010). Although an increase in synaptophysin-ir is not directly related to synaptogenesis, it might be suggested, based on the previously-described effects of FGF-2, that FGL plays a role in the development and formation of synapses; however further studies are necessary to explicitly examine this. Additionally, it is also important to note that changes in synaptophysin-ir (induced by FGL treatment) could reflect an alteration in the density of synaptic vesicles per synapse.

PSD-95-ir was decreased in the CA3 and DG of aged animals (Figure 1H). Treatment with FGL had no significant effect on PSD-95-ir in the CA3, DG or hilus, but somewhat unexpectedly, produced a slight reduction in PSD-95-ir in the CA1 of aged animals (Figure 1H). PSD-95 is localised predominantly in the postsynaptic density of asymmetric synapses and has an integral role in anchoring and organizing NMDA receptors and other proteins at the postsynaptic density (Hata and Takei, 1999; Kim and Sheng 2004; Sheng and Pak 1999). PSD-95 plays an important role in synaptic plasticity, through contributing to synaptic maturation and stabilization of excitatory synapses (El-Husseini et al., 2000). PSD-95, expressed on 60% of excitatory synapses (Aoki et al., 2001), is retained longer at the synapse with increasing age, with its levels determining synaptic size and strength (Gray et al., 2006). The selective age-related change in PSD-95-ir within the hippocampus (affecting the CA3 and DG) is intriguing. When compared with the more widespread loss of synaptophysin-ir, it could partially indicate an increased half-life for PSD-95, or its potential to be retained on synaptic membranes, but these are only speculative at present.

4.2. FGL effects on neuroglial-synaptic interactions

We noted an age-related reduction in the density of axo-spinous synapses within the CA3-SR at EM level (Figure 2B). These results are consistent with previous unbiased stereological studies (Adams et al., 2010; Geinisman et al., 1992) and corroborate the proposal that marked regional loss of synapses precedes gross neuronal loss in ageing. FGL treatment did not alter synaptic density within the CA3-SR, which was in agreement with our previous study, showing no effect on synapse number in the DG of aged animals treated with FGL (Popov et al., 2008).

Given the novel anti-inflammtory role of FGL, evidence indicating that FGL modulates glial cell activation (Downer et al. 2010), and that maintenance of neuroglial cells in a non-inflammatory ('quiescent') state could be an important determining factor for preserving synaptic function (Piazza

and Lynch, 2009), we wanted to investigate whether FGL directly affects glial-synaptic interaction at the EM level. Thus we proceeded to further determine the impact of ageing and FGL treatment on neuroglial-synaptic interaction within the CA3-SR.

Although there was no change in the surface area of astrocytic processes within the CA3-SR with age (Figure 3D), the mean numbers of astrocyte-synapse contacts were reduced by 2-fold (Figure 3E). This suggests that astrocytic support at the synapse is attenuated in aged rats and could be a key contributor towards impairment in synaptic connectivity, and brain cognitive capability. FGL increased synapse-astrocytic contacts in aged animals, restoring 'physical' astrocytic support at the synapse. Our studies also show that FGL treatment reduced astrocyte perimeter coverage of synapses in aged animals (Figure 3F). Astrocytes are known to control effectively the levels of glutamate following synaptic activity through glutamate transporters expressed at high density on their membrane processes (Diamond., 2005; Reichenbach et al., 2010; Witcher et al; 2007). It has been shown that the degree to which glutamate and other substances can escape or enter the perimeter of the synapse is dependent upon the length of astroglia-free interface (Witcher et al., 2007). A reduction in astrocytic coverage of synapses (following FGL treatment), could represent a 'compensatory' plastic change which would allow greater availability of glutamate between neighbouring synapses, which would, in effect serve to enhance synaptic function, demonstrated in behavioural *in vivo* studies (Klementiev et al., 2007).

In contrast, both the surface area of IBA1+ microglial processes and the mean number of microglia-synapse contacts were elevated in aged rats, within the CA3-SR, and these were attenuated following FGL treatment (Figure 4D,E). However, microglial coverage of synapses did not alter with age or FGL treatment (Figure 4F). Microglia vigilantly survey the microenvironment of the brain *in vivo* (Banati, 2003; Davalos et al., 2005) and their processes, like those of astrocytes, are found closely apposed to pre-and postsynaptic elements. They are vital sensors of pathological events in the brain and could potentially be activated by tagged/degenerating synapses (Bruce-Keller 1999, Krutzberg, 1996). A recent study (Wake et al., 2009) using two photon confocal imaging showed resting microglial processes making intimate but transient (4-5mins), direct contacts with healthy neuronal synapses. However in pathological settings (e.g. ischemic conditions) microglia-synapse contacts were shown to persist for over an hour with the subsequent disappearance of presynaptic boutons. Our morphometeric analyses indicate that microglial processes interact more frequently with synapses (microglia-synaptic contacts) in aged animals (Figure 4E). Morphologically, microglia in aged animals frequently displayed a higher content of intracellular vacuoles, phagolysosomal and electron-dense material, indicative of greater phagocytic activity, and an increased 'activation state'. Interestingly, the increase in microglial-synaptic contacts (Figure 4E) parallels the loss of synapses within CA3-SR (Figure 2B). Our data provide morphological evidence of increased contact between microglial processes at synapses within the

aged hippocampus. This could indicate reduced motility and/or an increased spatiotemporal interaction of microglia with synapses (Wake et al., 2009). These results can however, only be confirmed in live imaging (*in vivo*) studies, and further work will be needed to examine the dynamics of such interactions.

4.3. FGL effects on CD200-ir and cellular distribution

Interaction between CD200 and CD200R plays a role in maintaining microglia in a 'quiescent' state (Lyons et al., 2007). FGL peptide binds to FGF receptors which are known to be expressed on neurons, including within the hippocampus (e.g. FGFR1 and FGFR2; Gonzalez et al., 1995). Previous studies suggest that FGL promotes neuronal expression of CD200 *in vitro* (Downer et al. 2009), through an IL4-dependent mechanism (Downer et al., 2010). Varying CD200 expression levels will impact on the activation status of microglial cells (Kloss et al., 1997). We used an optical segmentation procedure to examine quantitatively the expression patterns of CD200-ir within hippocampal subfields. Aged animals showed a significant reduction in CD200-ir specifically within the CA3 and DG, with no notable change in CA1 or hilus (Figure 1I). Aged rats treated with FGL showed preservation of CD200-ir solely within the CA3 hippocampal subfield. Our results suggest differential age-related responses within subfields of the hippocampus, and point towards selective effects of FGL within the CA3 area. The age-related reduction in CD200-ir within the CA3 (Figure 1I) correlates with greater microglia-synaptic contacts and synaptophysin-ir within the CA3 in aged animals (Figure 4B). The reason for the differential responses within the subfields of the hippocampus is unknown. This could be due to the unique ability of the CA3 in displaying marked structural plasticity, which is accompanied by loss of hippocampal function (McEwen, 1999; Sandi et al., 2003; Sousa et al., 1998). To support this, microarray studies have revealed that age-related changes in expression of genes linked with cognition are affected more in the CA3 region compared to other subfields of the hippocampus (Haberman et al., 2009).

We turned to EM analyses, to examine the cellular distribution of CD200 in more detail, and determine whether CD200 might be mediating a modulatory effect at the synaptic level. Pre-embedding single immuno-DAB labelling showed selective expression of CD200 on boutons, axons, spines, dendrites and glial (astrocyte) processes. CD200 staining was noted on astrocytic end feet processes, and vascular endothelium (luminal aspect), the latter confirming a previous report by Ko et al. (2009). To date, most reports have emphasised a membrane-bound localisation for CD200 (Barclay et al., 2002; Lynch, 2010). We show that CD200 labelling is present both on membranes and intracellularly within neuronal and glial profiles. CD200 was prominently expressed on dendrites (50-75%) and on astrocytes (15-30%) (Figure 5I). By comparison, less than 12.5% of boutons (on a subset of synaptic vesicular membrane), axons and spines were found to express CD200 in the CA3-SR. These novel observations indicate that CD200 is at least partially associated

with the pre- and post-synaptic elements of the synapse, and imply that CD200 may have a role in regulating glial-synaptic interactions. Aged, vehicle-treated rats showed a 15% reduction in dendrites expressing CD200, compared to young vehicle-treated animals, but the distribution in spines, axons and astrocytes was elevated slightly with age (Figure 5I). FGL treatment increased slightly the CD200+ distribution in boutons and glial cell profiles, in aged (22 month-old) animals. This raises the possibility of an increased modulatory role of CD200, and enhanced glial support at the synapse, following FGL treatment.

Our findings provide evidence of marked age-related changes in synaptic proteins (synaptophysin and PSD-95), CD200 and glial-synaptic interactions within the hippocampus, and indicate that the NCAM-derived peptide, FGL, induces dynamic and adaptive changes in neuroglial-synaptic support probably by keeping glial cells in a non-inflammatory (quiescent) state. This is a role likely played through the ability of FGL to reverse the effect of aging on glial inhibitory factor (CD200).

References

Adams, M.M., Donohue, H.S., Linville, M.C., Iversen, E.A., Newton I.G., Brunso-Bechtold, J.K., 2010. Age-related synapse loss in hippocampal CA3 is not reversed by caloric restriction. Neuroscience. 171, 373-382.

Alder, J., Xie, Z.P., Valtorta, F., Greengard, P., Poo, M., 1992. Antibodies to synaptophysin interfere with transmitter secretion at neuromuscular synapses. Neuron. 9, 759-768.

Anand, R., Seiberling, M., Kamtchoua, T., Pokorny, R., 2007. Tolerability, safety and pharmacokinetics of the FGLL peptide, a novel mimetic of neural cell adhesion molecule, following intranasal administration in healthy volunteers. Clin. Pharmacokinet. 46, 351-358.

Aoki, C., Miko, I., Oviedo, H., Mikeladze-Dvali, T., Alexandre, L., Sweeney, N., Bredt, D.S., 2001. Electron microscopic immunocytochemical detection of PSD-95, PSD-93, SAP-102, and SAP-97 at postsynaptic, presynaptic, and nonsynaptic sites of adult and neonatal rat visual cortex. Synapse. 40, 239-257.

Banati, R.B., 2003. Neuropathological imaging: in vivo detection of glial activation as a measure of disease and adaptive change in the brain. Br. Med Bull. 65, 121-131.

Barclay, A.N., Wright, G.J., Brooke, G., Brown, M.H., 2002. CD200 and membrane protein interactions in the control of myeloid cells. Trends. Immunol. 23, 285-290.

Barres, B.A., 2008. The mystery and magic of glia: a perspective on their roles in health and disease. Neuron. 60, 430-440.

Berezin, V., Bock, E., 2010. NCAM mimetic peptides: an update. Adv. Exp. Med. Biol 663, 337-353.

Berezin, V., Bock, E., 2004. NCAM mimetic peptides: Pharmacological and therapeutic potential. J. Mol. Neurosci. 22, 33-39.

Berezin, V., Bock, E, Poulsen, F.M., 2000. The neural cell adhesion molecule. Curr Opin Drug Discov Devel. 3, 605-609.

Brey, E.M., Lalani, Z., Johnston, C., Wong, M., McIntire, L.V., Duke, P.J., Patrick, C.W.Jr., 2003. Automated selection of DAB-labeled tissue for immunohistochemical quantification. J. Histochem. Cytochem. 51, 575-584.

Bliss, T.V., Collingridge, G.L., 1993. A synaptic model of memory: long-term potentiation in the hippocampus. Nature. 361, 31-39..

Bondareff, W., Geinisman, Y., 1976. Loss of synapses in the dentate gyrus of the senescent rat. Am. J. Anat. 145, 129-136.

Bruce-Keller, A.J., 1999. Microglial-neuronal interactions in synaptic damage and recovery. J. Neurosci. Res. 58, 191-201.

Burke, S.N., Barnes, C.A., 2006. Neural plasticity in the ageing brain. Nat. Rev. Neurosci. 7, 30-40.
Cambon, K., Hansen, S.M., Venero, C., Herrero, A.I., Skibo, G., Berezin, V., Bock, E., Sandi, C., 2004. A synthetic neural cell adhesion molecule mimetic peptide promotes synaptogenesis, enhances presynaptic function, and facilitates memory consolidation. J. Neurosci. 24, 4197-204.
Campuzano, O., Castillo-Ruiz, M.M., Acarin, L., Castellano, B., Gonzalez, B., 2008. Distinct pattern of microglial response, cyclooxygenase-2, and inducible nitric oxide synthase expression in the aged rat brain after excitotoxic damage. J. Neurosci. Res. 86, 3170-3183.
Chitnis, T., Imitola, J., Wang, W., Elyaman, Y., Chawla, P., Sharuk, M., Raddassi, K., Bronson, R.T., Khoury, S.J., 2007. Elevated neuronal expression of CD200 protects Wlds mice from inflammation-mediated neurodegeneration. Am. J. Pathol. 170, 1695-1712.
C
Cuadrado, A., Nebreda, A.R., 2010. Mechanisms and functions of p38 MAPK signalling. Biochem. J. 429, 403-417.
Cullheim, S., Thams, S., 2007. The microglial networks of the brain and their role in neuronal network plasticity after lesion. Brain. Res. Rev. 55, 89-96.
Davalos, D., Grutzendler, J., Yang, G., Kim, J.V., Zuo, Y., Jung, S., Littman, D.R., Dustin M.L., Gan, W. B., 2005. ATP mediates rapid microglial response to local brain injury in vivo. Nat. Neurosci. 8, 752-758.
Davies, H.A., Kelly, A., Dhanrajan, T.M., Lynch, M.A., Rodriguez J.J., Stewart, M.G., 2003. Synaptophysin immunogold labelling of synapses decreases in dentate gyrus of the hippocampus of aged rats. Brain. Res. 986, 191-195.
Diamond, J.S., 2005. Deriving the glutamate clearance time course from transporter currents in CA1 hippocampal astrocytes: transmitter uptake gets faster during development. J. Neurosci. 25, 2906-2916.
Dobson, L., Conway, C., Hanley, A., Johnson, A., Costello, S., O'Grady, A., Connolly, Y., Magee, H., O'Shea, D., Jeffers, M., Kay, E., 2010. Image analysis as an adjunct to manual HER-2 immunohistochemical review: a diagnostic tool to standardize interpretation. Histopathology 57, 27-38.
Downer, E.J., Cowley, T.R., Cox, F., Maher, F.O., Berezin, V., Bock, E., Lynch, M.A., 2009. A synthetic NCAM-derived mimetic peptide, FGL, exerts anti-inflammatory properties via IGF-1 and interferon-gamma modulation. J. Neurochem. 109, 1516-1525.
Downer, E.J., Cowley, T.R., Lyons, A., Mills, K.H., Berezin, V., Bock, E., Lynch, M.A., 2010. A novel anti-inflammatory role of NCAM-derived mimetic peptide, FGL. Neurobiol. Aging. 31, 118-128.
Driscoll, I., Howard, S.R., Stone, J.C., Monfils, M.H., Tomanek, B., Brooks W.M., Sutherland, R.J., 2006. The aging hippocampus: a multi-level analysis in the rat. Neuroscience. 139, 1173-1185.
El-Husseini, A.E., Schnell, E., Chetkovich, D.M., Nicoll, R.A., Bredt, D.S., 2000. PSD-95 involvement in maturation of excitatory synapses. Science. 290, 1364-1368.
Evans, G.J., Cousin, M.A., 2005. Tyrosine phosphorylation of synaptophysin in synaptic vesicle recycling. Biochem. Soc. Trans. 33, 1350-1353.
Farber, K., Kettenmann, H., 2005. Physiology of microglial cells. Brain. Res. Brain. Res. Rev 48, 133-143.
Geinisman, Y., 1999. Discussion. Neurobiol. Aging. 20, 353-356.
Geinisman, Y., deToledo-Morrell, L., Morrell, F., Persina, I. S., Rossi, M., 1992. Age-related loss of axospinous synapses formed by two afferent systems in the rat dentate gyrus as revealed by the unbiased stereological dissector technique. Hippocampus 2, 437-444.
Geinisman, Y., Ganeshina, O., Yoshida, R., Berry, R.W., Disterhoft, J.F., Gallagher, M., 2004. Aging, spatial learning, and total synapse number in the rat CA1 stratum radiatum." Neurobiol. Aging. 25, 407-416.
Geinisman, Y., Morrell F., deToledo-Morrell, L., 1992. Increase in the number of axospinous synapses with segmented postsynaptic densities following hippocampal kindling. Brain. Res. 569, 341-347.

Geinisman, Y., de Toledo-Morrell, L., Morrell, F., 1986. Loss of perforated synapses in the dentate gyrus: morphological substrate of memory deficit in aged rats. Proc. Natl. Acad. Sci. U S A. 83, 3027-3031.

Giaume, C., Koulakoff, A., Roux, L., Holcman, H., Rouach, N., 2010. Astroglial networks: a step further in neuroglial and gliovascular interactions. Nat. Rev. Neurosci. 11, 87-99

Godbout, J.P., Chen, J., Abraham, J., Richwine, A.F., Berg, B.M., Kelley, K.W., Johnson, R.W., 2005. Exaggerated neuroinflammation and sickness behavior in aged mice following activation of the peripheral innate immune system. Faseb. J. 19, 1329-1331.

Gonzalez, A.M., Berry, M., Maher, P.A., Logan A., Baird, A., 1995. A comprehensive analysis of the distribution of FGF-2 and FGFR1 in the rat brain. Brain. Res. 701, 201-226.

Gray, N. W., Weimer, R.M., Bureau, I., Svoboda, K., 2006. Rapid redistribution of synaptic PSD-95 in the neocortex in vivo. PLoS. Biol. 4. e370.

Haberman, R.P., Colantuoni, C., Stocker, A.M., Schmidt, A.C., Pedersen J.T., Gallagher, M., 2009. Prominent hippocampal CA3 gene expression profile in neurocognitive aging. Neurobiol. Aging.

Hansen, S.M., Li, S., Bock, E., Berezin, V., 2010. Synthetic NCAM-derived ligands of the fibroblast growth factor receptor. Adv. Exp. Med. Biol. 663, 355-372.

Hata, Y., Takai, Y., 1999. Roles of postsynaptic density-95/synapse-associated protein 90 and its interacting proteins in the organization of synapses. Cell. Mol. Life. Sci 56, 461-472.

Jones, T.A., Greenough, W.T., 1996. Ultrastructural evidence for increased contact between astrocytes and synapses in rats reared in a complex environment. Neurobiol Learn. Mem. 65, 48-56.

Kim, E., Sheng, M., 2004. PDZ domain proteins of synapses. Nat. Rev. Neurosci. 5, 771-781.

Klementiev, B., Novikova, T., Novitskaya, V., Walmod, P.S., Dmytriyeva, O., Pakkenberg, B., Berezin, V., Bock, E., 2007. A neural cell adhesion molecule-derived peptide reduces neuropathological signs and cognitive impairment induced by Abeta25-35. Neuroscience. 145, 209-224.

Kloss, C.U., Kreutzberg G.W., Raivich, G., 1997. Proliferation of ramified microglia on an astrocyte monolayer: characterization of stimulatory and inhibitory cytokines. J. Neurosci. Res. 49, 248-254.

Ko, Y.C., Chien, H.F., Jiang-Shieh, Y.F., Chang, C.Y., Pai, M.H., Huang, J.P., Chen H.M., Wu, C.H., 2009. Endothelial CD200 is heterogeneously distributed, regulated and involved in immune cell-endothelium interactions. J. Anat. 214, 183-195.

Kokolakis, G., Panagis, L., Stathopoulos, E., Giannikaki, E., Tosca, A., Krüger-Krasagakis, S., 2008. From the protein to the graph: how to quantify immunohistochemistry staining of the skin using digital imaging. J. Immunol. Meth. 331, 140-146.

Leuba, G., Kraftsik, R., Saini, K., 1998. Quantitative distribution of parvalbumin, calretinin, and calbindin D-28k immunoreactive neurons in the visual cortex of normal and Alzheimer cases. Exp. Neurol. 152, 278-291.

Li, A.J., Suzuki, S., Suzuki, M., Mizukoshi, E., Imamura, T., 2002. Fibroblast growth factor-2 increases functional excitatory synapses on hippocampal neurons. Eur. J. Neurosci. 16, 1313-1324.

Lynch, A.M., Loane, D.J., Minogue, A.M., Clarke, R.M., Kilroy, D., Nally, R.E., Roche, O.J., O'Connell, F., Lynch, M.A., 2007. Eicosapentaenoic acid confers neuroprotection in the amyloid-beta challenged aged hippocampus. Neurobiol. Aging. 28, 845-855.

Lynch, A.M., Lynch, M.A., 2002. The age-related increase in IL-1 type I receptor in rat hippocampus is coupled with an increase in caspase-3 activation. Eur. J. Neurosci. 15, 1779-1788.

Lynch, M.A., 2009. The multifaceted profile of activated microglia. Mol. Neurobiol. 40, 139-156.

Lynch, M.A., 2010. Age-related neuroinflammatory changes negatively impact on neuronal function. Front. Aging. Neurosci 1, 6-22.

Lyons, A., Downer, E.J., Crotty, S., Nolan, Y.M., Mills K.H., Lynch, M.A., 2007. CD200 ligand receptor interaction modulates microglial activation in vivo and in vitro: a role for IL-4. J. Neurosci. 27, 8309-8313.

Lyons, A., Lynch, A.M., Downer, E.J., Hanley, R., O'Sullivan, J.B., Smith, A., Lynch, M.A., 2009. Fractalkine-induced activation of the phosphatidylinositol-3 kinase pathway attentuates microglial activation in vivo and in vitro. J. Neurochem. 110, 1547-1556.

McEwen, B.S., 1999. Stress and the aging hippocampus. Front Neuroendocrinol 20, 49-70.

Milnerwood, A.J., Cummings, D.M., Dallerac, G.M., Brown, J.Y., Vatsavayai, S.C., Hirst, M.C., Rezaie, P., Murphy, K.P., 2006. Early development of aberrant synaptic plasticity in a mouse model of Huntington's disease. Hum. Mol. Genet. 15, 1690-1703.

Mullany, P.M., Lynch, M.A., 1998. Evidence for a role for synaptophysin in expression of long-term potentiation in rat dentate gyrus. Neuroreport 9, 2489-2494.

Navone, F., Jahn, R., Di Gioia, G., Stukenbrok, H., Greengard, P., De Camilli., P., 1986. Protein p38: an integral membrane protein specific for small vesicles of neurons and neuroendocrine cells. J. Cell. Biol. 103, 2511-2527.

Neiiendam, J.L., Kohler, L.B., Christensen, C., Li, S., Pedersen, M.V., Ditlevsen, D.K., Kornum, M.K., Kiselyov, V.V., Berezin, V., Bock, E., 2004. An NCAM-derived FGF-receptor agonist, the FGL-peptide, induces neurite outgrowth and neuronal survival in primary rat neurons. J. Neurochem. 91, 920-935.

Paixao, S. Klein, R., 2010. Neuron-astrocyte communication and synaptic plasticity." Curr. Opin. Neurobiol. 20, 466-473.

Paxinos, G., Watson, C., 2007. The rat brain in stereotactic co-ordinates. Academic Press, 6th edition

Peddie, C.J., Davies, H.A., Colyer, F.M., Stewart, M.G., Rodriguez, J.J., 2008. Colocalisation of serotonin2A receptors with the glutamate receptor subunits NR1 and GluR2 in the dentate gyrus: an ultrastructural study of a modulatory role. Exp. Neurol. 211, 561-573.

Peters, A., Palay, S.L., Webster, H.D., 1991. The fine structure of the nervous system. Oxford UP, New York.

Piazza, A., Lynch, M.A., 2009. Neuroinflammatory changes increase the impact of stressors on neuronal function. Biochem. Soc. Trans. 37, 303-307..

Pontikis, C.C., Cella, C.V., Parihar, N., Lim, M.J., Chakrabarti, S., Mitchison, H.M., Mobley, W.C., Rezaie, P., Pearce D.A., Cooper, J.D., 2004. Late onset neurodegeneration in the Cln3-/- mouse model of juvenile neuronal ceroid lipofuscinosis is preceded by low level glial activation. Brain. Res. 1023, 231-242.

Popov, V.I., Medvedev, N.I., Kraev, I.V., Gabbott, P.L., Davies, H.A., Lynch, M., Cowley, T.R., Berezin, V., Bock, E., Stewart, M.G., 2008. A cell adhesion molecule mimetic, FGL peptide, induces alterations in synapse and dendritic spine structure in the dentate gyrus of aged rats: a three-dimensional ultrastructural study. Eur. J. Neurosci. 27, 301-314.

Popovich, P.G., Longbrake, E.E., 2008. Can the immune system be harnessed to repair the CNS? Nat. Rev. Neurosci. 9, 481-493.

Rapp, P.R., Gallagher, M., 1996. Preserved neuron number in the hippocampus of aged rats with spatial learning deficits. Proc. Natl. Acad. Sci. U S A. 93, 9926-9930.

Rehm, H., Wiedenmann, B., Betz, H., 1986. Molecular characterization of synaptophysin, a major calcium-binding protein of the synaptic vesicle membrane. Embo. J. 5, 535-541.

Reichenbach, A., Derouiche, A., Kirchhoff, F., 2010. Morphology and dynamics of perisynaptic glia. Brain. Res. Rev. 63, 11-25.

Rezaie, P., Pontikis, C.C., Hudson, L., Cairns N.J., Lantos, P.L., 2005. Expression of cellular prion protein in the frontal and occipital lobe in Alzheimer's disease, diffuse Lewy body disease, and in normal brain: an immunohistochemical study. J. Histochem. Cytochem. 53, 929-940.

Rodriguez J.J., Davies, H.A., Silva, A.T., De Souza, I.E., Peddie, C.J., Colyer, F.M., Lancashire, C.L., Fine, A., Errington, M.L., Bliss, T.V., Stewart, M.G., 2005. Long-term potentiation in the rat dentate gyrus is associated with enhanced Arc/Arg3.1 protein expression in spines, dendrites and glia. Eur. J. Neurosci. 21, 2384-2396.

Rosenzweig, E.S., Barnes, C.A., 2003. Impact of aging on hippocampal function: plasticity, network dynamics, and cognition. Prog. Neurobiol. 69, 143-179.

Sandi, C., Davies, H.A., Cordero, M.I., Rodriguez, J.J., Popov V.I., Stewart, M.G., 2003. Rapid reversal of stress induced loss of synapses in CA3 of rat hippocampus following water maze training. Eur. J. Neurosci. 17, 2447-2456.

Scheff, S.W., Price, D.A., Schmitt, F.A., Mufson, E.J., 2006. Hippocampal synaptic loss in early Alzheimer's disease and mild cognitive impairment. Neurobiol. Aging. 27, 1372-1384.

Schultz, R.L., Maynard, E.A., Pease, D.C., 1957. Electron microscopy of neurons and neuroglia of c,erebral cortex and corpus callosum. Am. J. Anat. 100, 369-407.

Secher, T., Novitskaia, V., Berezin, V., Bock, E., Glenthoj, B., Klementiev, B., 2006. A neural cell adhesion molecule-derived fibroblast growth factor receptor agonist, the FGL-peptide, promotes early postnatal sensorimotor development and enhances social memory retention. Neuroscience. 141, 1289-1299.

Sheng, M., Pak, D.T., 1999. Glutamate receptor anchoring proteins and the molecular organization of excitatory synapses. Ann. N. Y. Acad. Sci. 868, 483-493.

Skibo, G.G., Lushnikova, I.V., Voronin, K.Y., Dmitrieva, O., Novikova, T., Klementiev, B., Vaudano, E., Berezin, V.A., Bock, E., 2005. A synthetic NCAM-derived peptide, FGL, protects hippocampal neurons from ischemic insult both in vitro and in vivo. Eur. J. Neurosci. 22, 1589-1596.

Sousa, N., Almeida, O.F., Holsboer, F., Paula-Barbosa, M.M., Madeira, M.D., 1998. Maintenance of hippocampal cell numbers in young and aged rats submitted to chronic unpredictable stress. Comparison with the effects of corticosterone treatment. Stress. 2, 237-249.

Stewart, M., Popov, V., Medvedev, N., Gabbott, P., Corbett, N., Kraev, I., Davies, H., 2010 Dendritic spine and synapse morphological alterations induced by a neural cell adhesion molecule mimetic. Adv. Exp. Med. Biol. 663, 373-383.

Trapp, B.D., Wujek, J.R., Criste, G.A., Jalabi, W., Yin, X., Kidd, G.J., Stohlman, S., Ransohoff, R., 2007. Evidence for synaptic stripping by cortical microglia. Glia. 55, 360-368.

Tremblay, M.E., Lowery, R.L., Majewska, A.K., 2010. Microglial interactions with synapses are modulated by visual experience. PLos Biol. 8, 1-16.

Ventura, R., Harris, K.M., 1999. Three-dimensional relationships between hippocampal synapses and astrocytes. J. Neurosci. 19, 6897-6906.

Wake, H., Moorhouse, A.J., Jinno, S., Kohsaka, S., Nabekura, J., 2009. Resting microglia directly monitor the functional state of synapses in vivo and determine the fate of ischemic terminals. J. Neurosci. 29, 3974-3980.

Walmod, P.S., Kolkova, K., Berezin, V., Bock, E., 2004. Zippers make signals: NCAM-mediated molecular interactions and signal transduction. Neurochem. Res. 29, 2015-2035.

Wang, C.J., Zhou, Z.G., Holmqvist, A., Zhang, H., Li, Y., Adell, G., Sun, X.F., 2009. Survivin expression quantified by Image Pro-Plus compared with visual assessment. Appl. Immunohistochem. Mol. Morphol. 17, 530-535.

Witcher, M.R., Kirov, S.A., Harris, K.M., 2007. Plasticity of perisynaptic astroglia during synaptogenesis in the mature rat hippocampus. Glia. 55, 13-23.

Xavier, L.L., Viola, G.G., Ferraz, A.C., Da Cunha, C., Deonizio, J.M.D., Netto, C.A., Achaval, M., 2005. A simple and fast densitometric method for the analysis of tyrosine hydroxylase immunoreactivity in the substantia nigra pars compacta and in the ventral tegmental area. Brain Res. Prot. 16, 58-64.

Yamada, J., Hayashi, Y., Jinno, S., Wu, Z., Inoue, K., Kohsaka, S., Nakanishi, H., 2008. Reduced synaptic activity precedes synaptic stripping in vagal motoneurons after axotomy. Glia. 56, 1448-1462.

Zehntner, S.P., Chakravarty, M.M., Bolovan, R.J., Chan, C., Bedell, B.J., 2008. Synergistic tissue counterstaining and image segmentation techniques for accurate, quantitative immunohistochemistry. J. Histochem. Cytochem. 56, 873-880.

Zhang, J.M., Wang, H.K., Ye, C.Q., Ge, W., Chen, Y., Jiang, Z.L., Wu, C.P., Poo, M.M., Duan, S., 2003. ATP released by astrocytes mediates glutamatergic activity-dependent heterosynaptic suppression. Neuron. 40, 971-982.

FIGURE LEGENDS

Figure 1. Synaptophysin, PSD-95 and CD200 immunoreactivity within the hippocampus of young (4 month-old) and aged (22 month-old) rats treated with vehicle or FGL.
(**A-D**): Micrographs showing immunoreactivity (-ir) for synaptophysin (A,B), PSD-95 (C,D) and CD200 in the CA1 (A,C,E) and CA3 (B,D,F) subfields of the hippocampus. Inset figures show immunostaining associated with pyramidal cell somata at higher magnification for each marker. (**G-I**): Quantitative analysis of synaptophysin-ir, PSD-95-ir and CD200-ir within the hippocampus of young (4 month) and aged (22 month) rats treated with vehicle, and with FGL at 22 months. Graphs show the mean percentage immunoreactivity (% Area) per microscopic field, determined by optical segmentation (as outlined in the Materials and Methods). Aged vehicle-treated rats showed a significant reduction in synaptophysin-ir within all subfields of the dorsal hippocampus (CA1, CA3, DG and hilus), compared to younger vehicle-treated rats (G). Note the comparatively low levels of synaptophysin-ir detected within the CA1 area (A,G). PSD95-ir and CD200-ir were significantly reduced with age only in the CA3 and DG (H,I). FGL treatment moderately preserved synaptophysin-ir within the CA3 and hilus (G), and CD200-ir (I) only within the CA3, but had no major effect on PSD-95-ir (except for a small decline within the CA1 subfield) in aged (22 month-old) animals. These results indicate differential age-related responses between the CA1 and CA3 subfields of the hippocampus, and point towards selective effects of FGL within the CA3 area. Abbreviations: CA1-SP (hippocampal CA1 stratum pyramidal area), CA1-SR (hippocampal CA1 stratum radiatum area), CA3-SP (hippocampal CA3 stratum pyramidal area), CA3-SR (hippocampal CA3 stratum radiatum area), DG (dentate gyrus of the hippocampus), Total (mean total hippocampal value). Data are plotted as mean values ± SEM (n=5 animals per group). A minimum of 20 individual microscopic fields were analysed per region, per animal (see Methods), Asterisks denote statistical significance: (*) $p<0.05$, (**) $p<0.01$, (***) $p<0.001$. Scale bar in (F) represents 41μm in (A-F).

Figure 2. Synaptic density within the CA3 (stratum radiatum) of young (4 month-old) and aged (22 month-old) rats treated with vehicle or FGL.
(**A**) Electron micrograph showing axo-spinous synapses within the neuropil of the CA3-SR (white arrows). (**B**) Graph showing mean number of synapses per 100μm² in the CA3-SR of young (4 month) and aged (22 month) vehicle-treated rats, and aged rats treated with FGL. The mean number of synapses is reduced with age, and remains unaffected by treatment with FGL. Abbreviation: CA3-SR (hippocampal CA3 stratum radiatum). Data plotted as mean values per 100μm² ± SEM (n=4 animals per group). A minimum of 40 random (non-overlapping) EM fields, were analysed within the CA3-SR per animal (see Methods). Asterisks denote statistical significance: (***) $p<0.001$. Scale bar represents 1.23μm in (A).

Figure 3. Astrocyte-synaptic interactions within the CA3 (stratum radiatum) of young (4 month-old) and aged (22 month-old) rats treated with vehicle or FGL.
(**A-C**): Electron micrographs showing GFAP+ astrocyte processes (detected using pre-embedding immuno-EM (DAB) labelling with an antibody to GFAP); pseudocoloured in blue for emphasis. (**A**) An astrocyte process makes contact with several synapses (white arrows). (**B**) Higher power micrograph showing astrocytic contact/coverage at an axo-spinous synapse. (**C**) Lipofuscin can occasionally be detected within astrocyte processes in aged animals. (**D-F**): Quantitative analysis in 2D, of mean surface area of astrocyte processes (**D**), number of astrocyte-synapse contacts (**E**) and astrocytic coverage of synapses (**F**) within the CA3-SR of young (4 month) and aged (22 month) rats treated with vehicle, and with FGL at 22 months. The mean surface area of astrocyte processes, and coverage of synapses did not alter with age (**D,F**), whereas the mean number of astrocyte-synaptic contacts were significantly reduced in aged animals (**E**). FGL treatment further reduced astrocytic coverage of synapses (**F**), but increased the mean number of astrocyte-synaptic contacts (E) within the CA3-SR in aged animals (when compared to vehicle-treated animals). Abbreviations: (Ast) Astrocytic process, (s) Spine, (b) Bouton, (Lpf) Lipofuscin. CA3-SR (hippocampal CA3

stratum radiatum). Data are plotted as mean values ± SEM (n=4 animals per group). A minimum of 40 random (non-overlapping) EM fields, were analysed within the CA3-SR per animal (see Methods). Asterisks denote statistical significance: (**) $p<0.01$, (***) $p<0.001$. Scale bar in (A) represents 0.94µm in (A) and 2µm in (B) and (C).

Figure 4. Microglia-synaptic interactions within the CA3 (stratum radiatum) of young (4 month-old) and aged (22 month-old) rats treated with vehicle or FGL.
(**A-C**): Electron micrograph showing IBA-1+ microglial cells/processes (detected using pre-embedding immuno-EM (DAB) labelling with an antibody to IBA-1). (**A**) Microglial cell body and processes (delineated with a green marker) within the CA3-SR. The inset is a higher power micrograph showing the process segment from (**A**) pseudocoloured in yellow for emphasis, associated with a synapse (surface contact delineated in green on the inset) within the neuropil. (**B,C**): Age-related changes in the ultrastructural morphology of microglia within the CA3-SR. IBA-1+ microglial cells at 4 months (**B**) and 22 months (**C**). Microglia in aged animals frequently display a higher content of intracellular vacuoles, phagolysosomal and electron-dense material (indicative of greater phagocytic activity, and an increased 'activation state') (compare C to B). (**D-F**): Quantitative analysis in 2D, of mean surface area of microglial processes (**D**), number of microglia-synapse contacts (**E**) and microglial coverage of synapses (**F**) within the CA3-SR of young (4 month) and aged (22 month) rats treated with vehicle, and with FGL at 22 months. The mean surface area of microglial processes (**D**) and number of microglia-synapse contacts (**E**) increased significantly with age, but the microglial coverage of synapses remained unaltered (either with age, or following FGL treatment) (**F**). FGL treatment significantly reduced the mean surface area of microglial processes (**D**) and the mean number of microglia-synapse contacts (**E**) within the CA3-SR in aged animals (when compared to vehicle-treated animals). Abbreviations: (Mcg) microglia, (Lys) lysosome, (Lpf) Lipofuscin, CA3-SR (hippocampal CA3 stratum radiatum). Data are plotted as mean values ± SEM (n=4 animals per group). A minimum of 40 random (non-overlapping) EM fields, were analysed within the CA3-SR per animal (see Methods). Asterisks denote statistical significance as follows: (**) $p<0.01$, (***) $p<0.001$. Scale bar in (A), (B) and (C) represents 1.25µm (~2µm in the inset).

Figure 5. Cellular distribution of CD200 examined at EM level
(A-H): Electron micrographs showing CD200 localisation at the ultratructural level within the CA3-SR (detected using pre-embedding immuno-EM (DAB) labelling with an antibody to CD200). CD200 was not solely confined to neuronal cell membranes. Instead, CD200 appeared to be distributed differentially in glial cells (astrocytes), endothelial cells and neurons, and on various cellular profiles (with membrane-bound and intracellular patterns of expression) (**A**), including on vascular endothelium (luminal aspect of capillary endothelial cells (closed arrows), and vesicular membrane 'buds' (open arrows) (**B**), and astrocytic end-feet processes (emphasised by blue pseudocolour) (**B**), on synaptic boutons (vesicle membranes) (**C**), axons (**D**), spines (**E**), dendrites (**F**) and glial cell processes (**G,H**). Quantitative data showing the percentage distribution of CD200 (per 100µm²) amongst neuronal and glial profiles is presented in (**I**), within the CA3-SR of young (4 month) and aged (22 month) rats treated with vehicle, and with FGL at 22 months. CD200 was prominently expressed on dendrites (50-75%) and on astrocytes (15-30%) (**I**). By comparison, less than 12.5% of boutons, axons and spines were found to express CD200 in the CA3-SR. Aged vehicle-treated rats showed a 15% reduction in dendrites expressing CD200, compared to young vehicle-treated animals, but the distribution amongst spines, axons and astrocytes was elevated slightly with age (**I**). FGL treatment increased slightly the CD200+ distribution in boutons and glial cell profiles, in aged (22 month-old) animals. Abbreviations: Astrocyte processes (Ast), Spines (S), Axons (Ax), Boutons (B), Dendrites (D). A minimum of 40 random (non-overlapping) EM fields, were analysed within the CA3-SR per animal (see Methods). Scale bar in (A) represents 1.25µm in (A), 5µm in (B) and 2µm in (C-H).

Fig 1

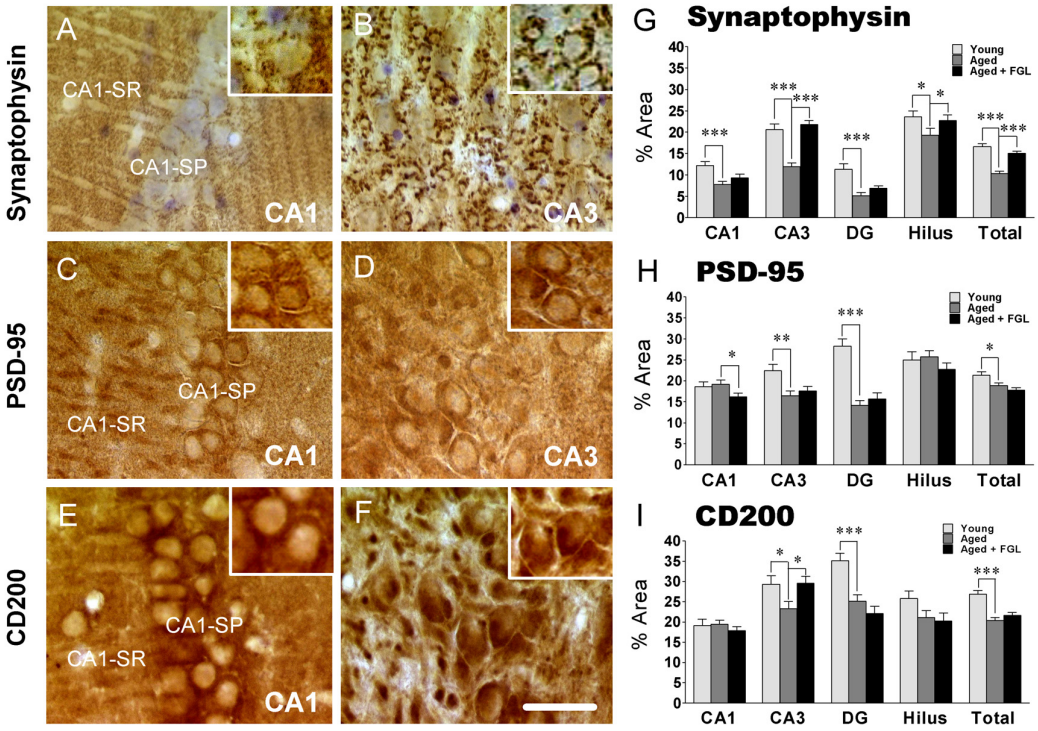

Fig 2

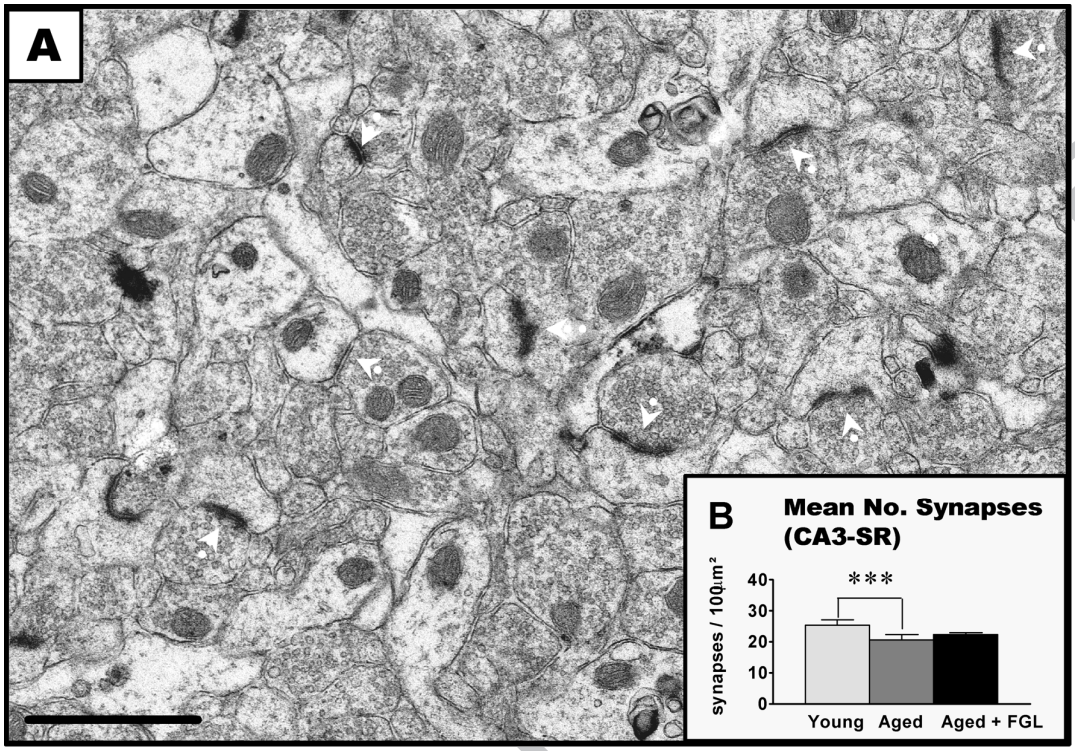

Fig 3

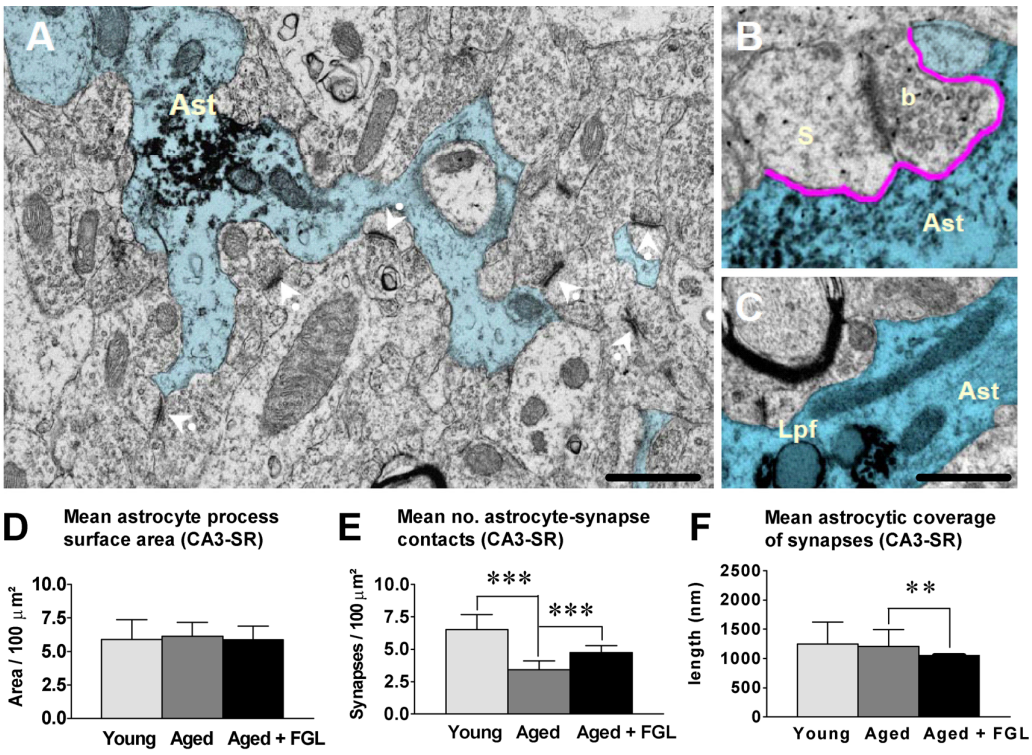

Fig 4

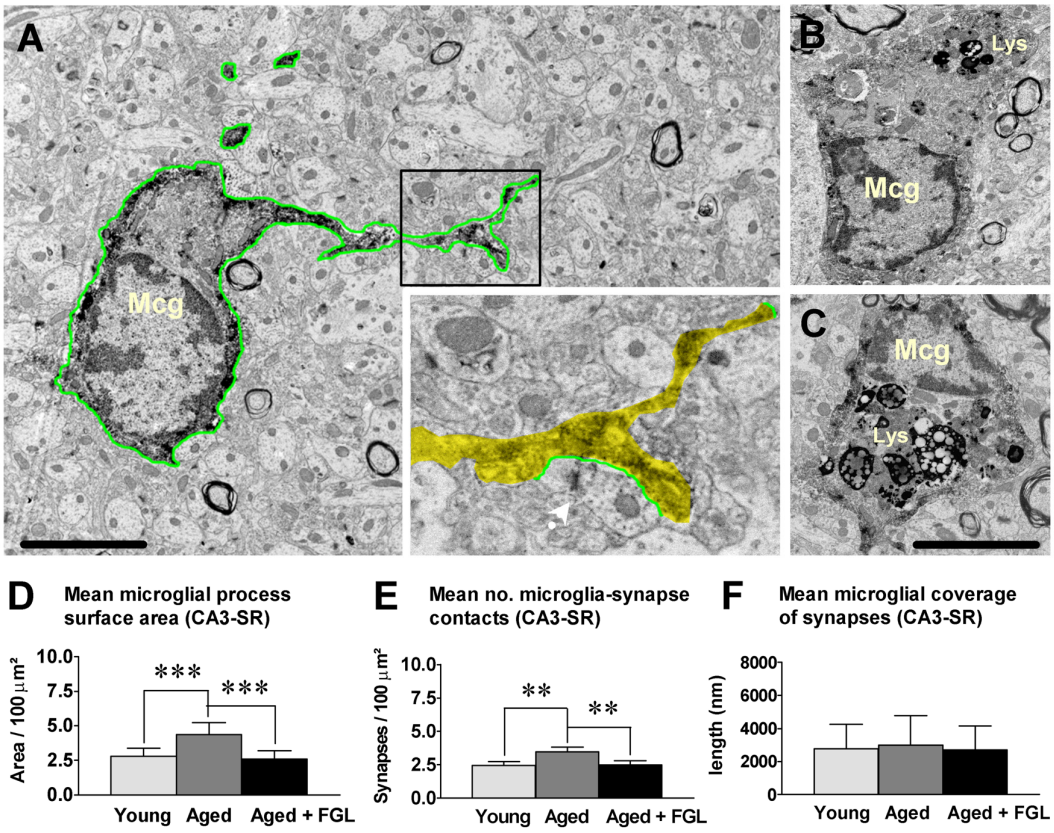

Fig 5

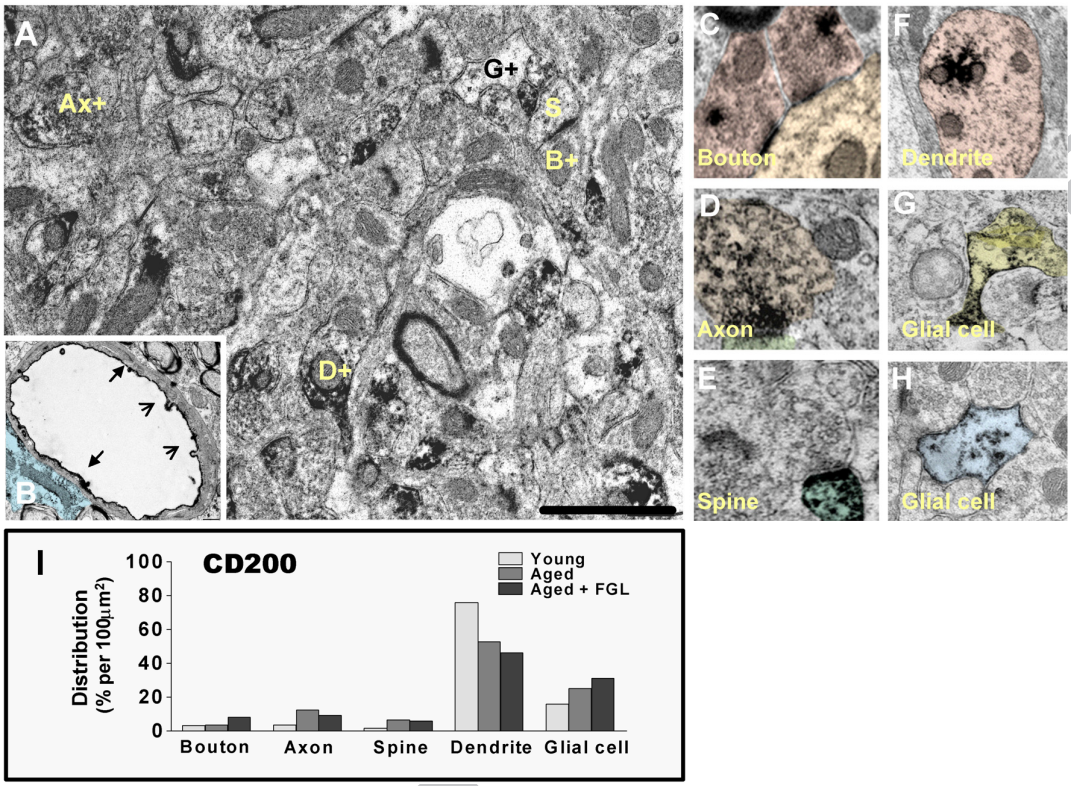

Highlights

Hippocampal age-related reductions in astrocyte-synaptic contacts, and increases in microglia-synaptic contacts were attenuated using the NCAM derived peptide, FGL